CEAS-GNC-2022-038

CEAS EuroGNC 2022
"Conference on Guidance, Navigation and Control"
3-5 May 2022 @ Technische Universität Berlin, Germany

IMU-based Aircraft Ground Tracking using Strapdown Integration, Vibration deduced Speed Estimation and Particle Filtering

Mats Martens Research Assistant, Technische Universität Berlin, Chair of Flight Guidance and Air Transport, 10587, Berlin, Germany. martens@tu-berlin.de

ABSTRACT

This work shows methods in the field of inertial sensor fusion and additional engineering knowledge to follow the position of an aircraft on the airport tarmac. Strapdown Integration is used to retrieve the drift affected position estimate of the aircraft from accelerometer and gyroscope data. The accelerometer data is used again to perform a vibration analysis using Power Spectral Density (PSD) and Root Mean Square (RMS) within the frequency band between 10Hz and 250Hz. By splitting the dataset into a reference and a test dataset, this yields a speed estimate based on the reference dataset. The Strapdown Integration based velocity estimate and the vibration deduced speed estimate are fused by a complementary filter. Furthermore, Zero Velocity Update reduces the effect of bias instability. Finally, knowing that aircraft under normal operation remain on the airport tarmac, a bootstrap particle filter exploits this additional knowledge of the airport layout. On the test dataset, the continuously rising position estimation error of the route, based on the fused speed and a linear kinematic model, was outperformed by the bootstrap particle filter.

Keywords: Taxi Guidance, Inertial Sensors, Particle Filter, Vibration Analysis, Velocity Estimation

Nomenclature

v_{acc}	=	Accelerometer based velocity estimate
v_{vib}	=	Vibration based velocity estimate
v_{fused}	=	Complementary filter based speed fusion of v_{vib} and v_{acc}
$\omega^b_{ib,t}$	=	Gyroscope measurement in the body frame
$f^b_{ib,t}$	=	Accelerometer measurement in the body frame
${}^e_b q_t$	=	Orientation of the body frame in the earth frame
P_{rms}	=	Root Mean Square of the Power Spectral Density

1 Introduction

Aircraft estimate their position based on combinations of different navigation systems. For Area Navigation (RNAV), aircraft rely on VHF Omni-directional Range (VOR), Distance Measuring Equipment (DME) and other radio navigation systems since the 1970s [1]. Additionally, inertial reference units are used to measure accelerations and angular rates. Further guidance was introduced with the availability of the Global Positioning System (GPS) [1].

Within the Advanced Surface Movement Guidance and Control Systems (A-SMGCS) Manual [2], the International Civil Aviation Organization (ICAO) finds, that currently aircraft movement on the tarmac is based on visual cues only. The manual defines a baseline for future developments to assist pilots, especially under low visibility operations. Localization with Global Navigation Satellite Systems (GNSS), such as GPS, suffers from multipath effects, i.e. reflection and diffraction of the radio signals, which is more likely in unfavorable environments such as close to buildings [3]. As the A-SMGCS Manual sets accuracy, integrity and continuity requirements, sensor fusion or alternative navigation techniques can help to improve the position estimation once the GNSS based position estimation is deteriorated.

This work introduces a position estimation approach of aircraft on ground, only relying on IMU data and knowledge of the airport layout. Hereby, the emphasis is on correcting the velocity estimate based on the IMU's mechanization equations by a speed estimator that uses the same measurements.

2 Reference Data Set

To evaluate the various techniques explained in the remainder of this paper, we make use of a data set that we collected. The whole data set consists of six data recordings of flights conducted on a Boeing 737-800. A custom-made data collection board was developed using a MEMS-grade InvenSense MPU9250 Inertial Measurement Unit (IMU) and the u-blox EVA-7M SiP GPS receiver, and rigidly attached to the aircraft structure on the flight deck. During the flights, all data was stored on an SD card. All recordings include the time, three-dimensional (3D) accelerometer readings, 3D gyroscope readings, 3D magnetometer readings and the GPS time and position. Except for the GPS data, all measurements are obtained at a data rate of 1.25kHz, whereas the GPS is recorded at a frequency of 0.5Hz. For the purpose of ground tracking only the taxi phases (movement on ground) of each flight from parking position to the runway are analyzed in detail. Five flights form the reference data set for the analysis of the sixth recording, which acts as test data set.

3 Methods and Algorithms

An overview of the following process is given in Figure 1. The reference data set is used to derive a speed predictor based on the vibration spectrum of the vertical channel of the measured accelerations. Using this speed predictor, Strapdown Integration and Zero Velocity Update, the test data set is processed. With the additional information of the tarmac layout using an airport map, a particle filter is used to determine a position estimate.

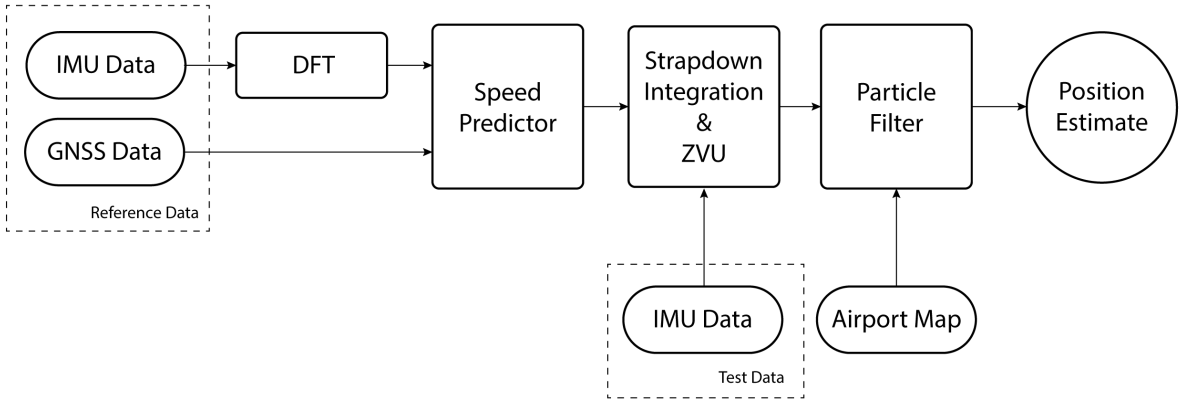

Fig. 1 Schematic Overview of the Applied Methods

3.1 Aircraft Kinematics

The landing gear of the Boeing 737-800 consists of a main landing gear of two wheels located left and right under the wing, and a nose gear following the configuration shown in Figure 2. As the nose gear can be steered and each wheel can rotate at a different rate, the motion of the aircraft on the ground has two degrees of freedom; the longitudinal movement and rotation around the vertical axis.

Effects of transverse velocity of the tires (drifting) are neglected. However, due to the lever arm between the center of rotation and the location of our sensors on the flight deck, a transverse velocity could be measured. As shown for tricycle wheeled robots by Siegwart [4], transverse acceleration and velocity can be neglected when mathematically moving the sensor to the center between both wheels of the main landing gear.

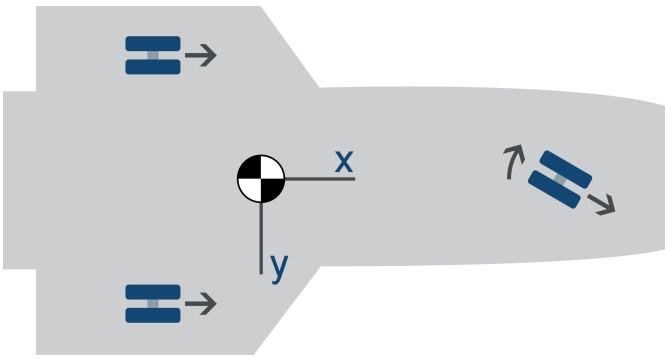

Fig. 2 Aircraft Landing Gear - Wheel Configuration and Coordinate System of the Body Frame b

3.2 Orientation Estimation

Before taxiing, the aircraft is at rest for at least 30 seconds during which the gyroscope turn-on bias is estimated by calculating the mean ω_μ of all three dimensional gyroscope measurements during this interval. This mean is then used to compensate the gyroscope measurements for each time step t by subtracting it from the measurements $\tilde{\omega}^b_{ib,t}$

$$\omega^b_{ib,t} = \tilde{\omega}^b_{ib,t} - \omega_\mu, \tag{1}$$

where ω^b_{ib} is the angular rate measurement of the body frame b relative to the inertial frame i expressed in the body frame. The measurement error model for a typical low-cost gyroscope follows an angular random walk [5]. In case of our gyroscope sensor the angular random walk error is approximately $0.04°/\sqrt{s}$. The average taxi duration of the recorded flights is 9.5 minutes and the maximum duration is 16 minutes. Therefore, in the worst case our error grows to about 1.2° after 16 minutes.

Given the a priori known initial heading, roll and pitch and the sampling frequency f_s, the orientation of the body frame is given as the quaternion ${}^e_b q_t$, which is expressed in the earth frame e. Each time step the orientation is updated using the integrated gyroscope measurement $\omega^b_{ib,t}$

$${}^e_b q_t = {}^e_b q_{t-1} \otimes \{\|\omega^b_{ib,t}\| \frac{1}{f_s} @ \frac{\omega^b_{ib,t}}{\|\omega^b_{ib,t}\|}\}, \tag{2}$$

where $\otimes$ is the quaternion multiplication operator and the notation $\{\alpha @ v\}$ represents a rotation quaternion with an angle α around the axis v. As a low cost IMU was used, the earth rotation rate was neglected.

Using the orientation of the body frame relative to the earth frame ${}^{e}_{b}q_t$, which is obtained from the previous equation, the body frame accelerometer measurements $f^{b}_{ib,t}$ can be rotated into the earth frame by applying

$$f^{e}_{ib,t} = {}^{e}_{b}q_t \otimes f^{b}_{ib,t} \otimes ({}^{e}_{b}q_t)^{-1}. \tag{3}$$

3.3 Velocity Estimation

3.3.1 Velocity Bias Compensation

Analogous to the gyroscope-bias compensation of the gyroscope in Section 3.2, the accelerometer bias can also be estimated from the mean acceleration measurement vector for the samples collected during the resting period and subtracted from all measurements. Note that the z-component, here, includes the reactive force of the gravity that must be subtracted as well. However, this effect is minimal if the inertial sensor's x- and y-axes are locally level. Since we are mostly interested in the ground velocity only both horizontal accelerations are used and integrated.

3.3.2 Vibration

In the field of automotive systems Lindfors et.al. proposed the use of vibration measurements to estimate the velocity of a vehicle [6]. They measured the characteristic frequencies of a car chassis and found a correlation with the speed of the car.

This paper focuses on the energy of vibration, which can be characterized by the Root Mean Square (RMS) of the signal's Power Spectral Density (PSD). Let the complex samples $X_k := X_0, ..., X_{N-1}$ represent the Discrete Fourier Transformation (DFT) of a signal as a function of frequency $f_k = k/N$, then the PSD $\tilde{P}$ is given by:

$$\tilde{P}(f_k) = \frac{1}{N} |X_k|^2 . \tag{4}$$

The use of RMS is a common method to measure the energy of random vibrations. For discrete PSD values it is defined as follows [7]:

$$P_{rms} = \sqrt{\frac{1}{N} \sum_{k=0}^{N-1} P_k} \tag{5}$$

For the first five recordings, the P_{rms} value of the acceleration vector is calculated on the interval from 10Hz to 250Hz for each point in time. Then, the velocity for each of the time epochs is derived from consecutive GPS positions and its horizontal norm, the ground speed, is mapped against calculated PSD values. Next, the relationship between ground speed and the vibration, as modeled by the PSD, is modeled as a quadratic regression. The results of this mapping and regression are shown in Figure 3 as are the velocity estimation errors. One can observe that the regression has an error below $2m/s$.

Then, the speed estimation of the test data set v_{vib} is calculated by evaluating the second order polynomial based on the coefficients from the regression of the reference data set.

3.3.3 Zero Velocity Update

Accelerometer biases change over time which leads to a growth of the velocity estimation error. To compensate for that growth, periods of rest can be used to estimate the accelerometer bias or velocity

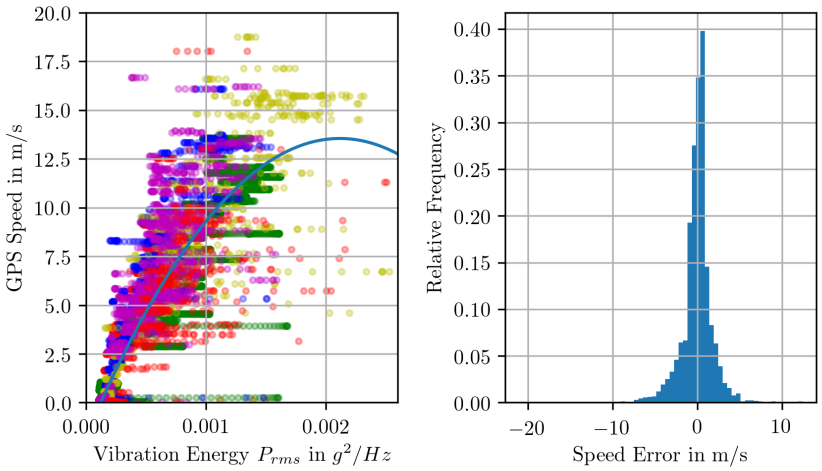

Fig. 3 Scatter Plot of Vibration and Velocity of Different Recordings Shown with Different Color (Left) and Histogram of the Error of a Quadratic Regression (Right)

drift (i.e. zero-velocity update). The introduced P_{rms} value is used to identify intervals in the recording showing a vibration lower than $2 \times 10^{-4} g^2/Hz$, which is a manually chosen value to match the resting periods of the reference data set. For each of these zero velocity intervals, the affine linear function $v_\Delta(t)$ between the previous resting period at time t_A and the start of the next period t_B is calculated as

$$v_\Delta(t) = \frac{v(t_B) - v(t_A)}{t_B - t_A}(t - t_A), \forall t \varepsilon [t_A, t_B] \tag{6}$$

.

The velocity estimates $v_{acc}(t)$ are them compensated for the estimated accelerometer bias by subtracting the drift estimate as

$$v_{acc,ZVU}(t) = v_{acc}(t) - v_\Delta(t), \forall t \varepsilon [t_A, t_B]. \tag{7}$$

3.3.4 Speed Fusion

After compensation of the accelerometer measurements using the zero-velocity update derived in Section 3.3.3, the measurements are considered bias compensated. Therefore, the underlying error distribution is considered zero-mean Gaussian.

The velocity estimate derived from our MEMS accelerometer shows a typical standard deviation of $2.7 m/s/\sqrt{h}$ since the last zero-velocity update [8]. By multiplying that value with the square root of the duration since the last update, the standard deviation of the accelerometer based velocity σ_{acc} is described. For the longest recording this error would increase to $1.4 m/s$. Now, the velocity estimate from the IMU, v_{acc}, and the estimate from the vibration-based estimator, v_{vib}, can be fused using a complementary filter weighted by factor α [9]. It is defined as

$$\alpha(t) = \frac{\sigma_{vib}^2}{\sigma_{vib}^2 + \sigma_{acc}^2(t)}, \tag{8}$$

where σ_{vib} is the standard deviation of the derived vibration based speed estimator. The fused speed is then calculated as

$$v_{fused}(t) = \alpha(t) \cdot v_{vib}(t) + (1 - \alpha(t)) \cdot \|v_{acc,ZVU}(t)\|. \tag{9}$$

The results of the fused speed estimation v_{fused} are shown in Figure 4 and compared to the GPS-based speed estimates. As shown in Section 3.1, no transversal velocity is possible and the fused speed is considered to act longitudinal only.

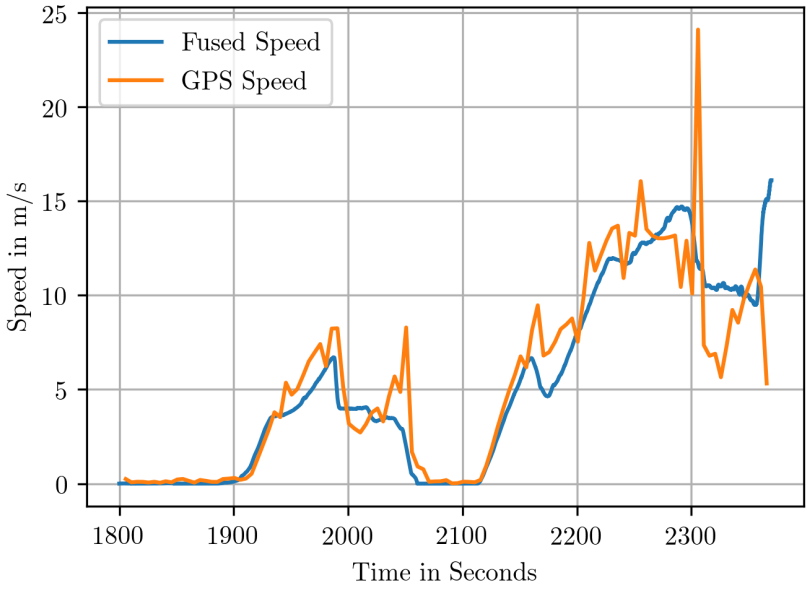

Fig. 4 Fused Ground Speed in Comparison to the Ground Truth GPS Ground Speed

3.4 Position Estimation

Next, the position is estimated using the *a priori* known initial position of the aircraft and the fused velocity v_{fused} by assuming the integration as

$$x_t = x_{t-1} + v_{fused,t} \cdot \frac{1}{f_s}. \tag{10}$$

Comparison of this position estimation to the actual position, the blue line in Figure 6, shows an error that grows over time to an error of approximately 1.25km. This error can be attributed to unresolved biases in the velocity estimates that are integrated in the position estimator.

3.4.1 Bootstrap Particle Filter

To reduce the error in the position estimate, additional knowledge is used. Under normal operations, an aircraft must always remain on the airport tarmac. Therefore, the area of possible position estimates is limited to that surface. Using a bootstrap particle filter, this additional knowledge can be exploited.

A particle filter algorithm is described by Thrun in [10] where he defines the filter to approximate the a posteriori distribution of the aircraft location given the inputs to the estimator (derived in previous sections). The M particles at the current time-epoch

$$X_t := x_t^{[1]}, \ldots, x_t^{[M]} \tag{11}$$

are generated based on the transition prior probability density

$$x_t^{[m]} \sim p(x_t | x_{t-1}^{[m]}). \tag{12}$$

The probability density function is a two dimensional multivariate Gaussian distribution formed by velocity and angular rate uncertainties. The measured position z_t is used to obtain importance factors or weights $\omega_t^{[m]}$ for each of the particles:

$$\overline{\omega}_t^{[m]} = p(z_t | x_t^{[m]}) \tag{13}$$

The likelihood function $p(z_t | x_t^{[m]})$ is now defined such that it includes knowledge of the airport layout. Those particles being off the airport surface are unlikely, the particles that are on tarmac are weighted more the closer they are to the measurement:

$$\overline{\omega}_t^{[m]} = \begin{cases} 1/\|x_t^{[m]} - z_t\| & \text{if } x_t^{[m]} \text{ on tarmac} \\ 0 & \text{otherwise} \end{cases} \tag{14}$$

The weights $\overline{\omega}_t^{[m]}$ are normalized. Calculating the weighted average of all particles, called centroid, gives the approximate position of the aircraft.

4 Results

As shown in Figure 5, off tarmac particles are identified by a darker color and correspond to low likely positions. Particles (i.e. possible positions) nearer to the actual path appear brighter, which indicates a high likelihood. The centroids are following the center line of the taxiway.

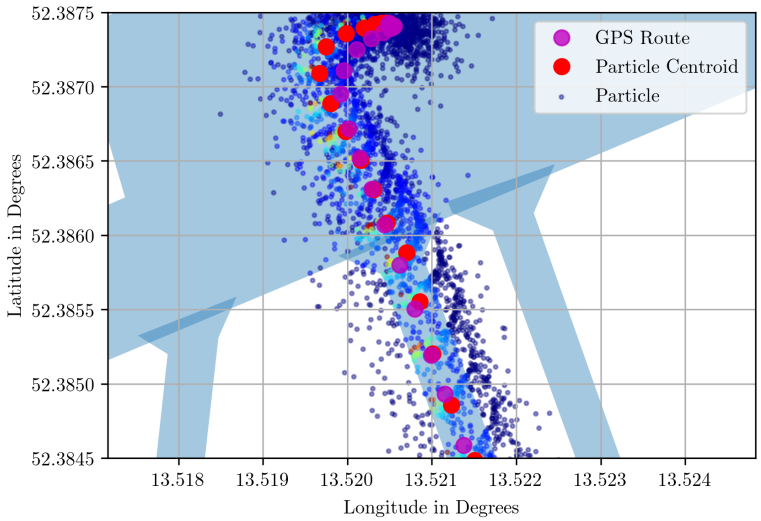

Fig. 5 Particle Filter - Particles of Multiple Iterations and Corresponding Centroids; 200 Particles per Iteration; Data Divided into 5 Seconds Subsets

The position estimation error over time is shown in Figure 6. It can be observed that, in contrast to the fused velocity integration, the particle filter estimation error is not continuously growing.

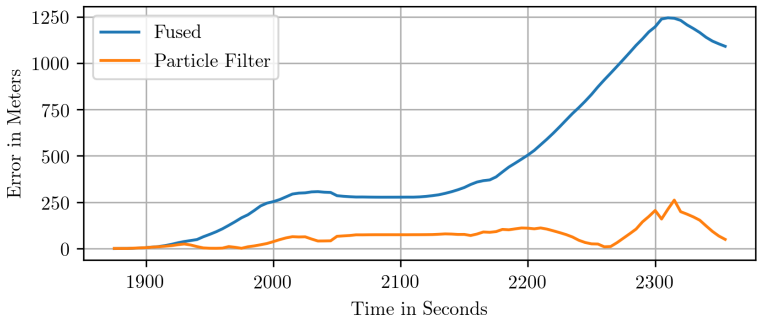

Fig. 6 Error of Position Estimation only based on Speed Fusion and the Bootstrap Particle Filter

5 Interpretation and Conclusions

This paper proposes an approach of smoothing IMU data to localize aircraft during ground movements. In a first step zero-velocity update yielded a good velocity estimate based on the raw IMU measurements. Additionally, a correlation between the vibration spectrum of the vertical accelerometer channel and the ground speed of the aircraft was found by comparing it to the GPS based ground speed. The complementary fusion of both velocity estimates resulted in a good combined estimate. However, by assuming a linear kinematic model, the aircraft position drift increased due to the integration of velocity errors. Finally, to compensate for that drift, a bootstrap particle filter was designed to incorporate the knowledge of the airport tarmac layout. Even though modern aircraft don't rely on low-cost IMUs, this paper demonstrated a method to correct IMU mechanized velocity estimates with vibration deduced estimates based on the same data. Using the Bootstrap Particle Filter, the position error could also be reduced significantly.

References

[1] Myron Kayton and Walter R. Fried. *Avionics Navigation Systems*. John Wiley & Sons, Inc., New York, 2 edition, 1997.

[2] International Civil Aviation Organization, The address of the publisher. *Advanced Surface Movement Guidance and Control Systems (A-SMGCS) Manual*, 1 edition, 2004. Doc 9830 AN/452.

[3] Michael S. Braasch. Multipath. In Peter J.G. Teunissen and Oliver Montenbruck, editors, *Handbook of Global Navigation Satellite Systems*, pages 443–468. Springer International Publishing, 2017.

[4] Roland Siegwart, Illah R. Nourbakhsh, and Davide Scaramuzza. *Introduction to Autonomous Mobile Robots, 2nd Edition*. The MIT Press, Cambridge, Massachusetts, 2011.

[5] Meron Gessesse and Mohamed Atia. Multi-sensor attitude and heading reference system using genetically optimized kalman filter. In *2018 IEEE 61st International Midwest Symposium on Circuits and Systems (MWSCAS)*. IEEE, 09 2018. DOI: 10.1109/MWSCAS.2018.8623949.

[6] Martin Lindfors, Gustaf Hendeby, Fredrik Gustafsson, and Rickard Karlsson. Vehicle speed tracking using chassis vibrations. In *2016 IEEE Intelligent Vehicles Symposium (IV)*. IEEE, 06 2016. DOI: 10.1109/IVS.2016.7535388.

[7] Christian Lalanne. *Mechanical Vibrations and Shock Analysis, Volume 3, Random Vibration, 3rd Edition*. John Wiley & Sons, Inc, 111 River Street, Hoboken, NJ 07030, USA, 2014.

[8] Quan Zhang, Xiaoji Niu, Hongping Zhang, and Chuang Shi. Algorithm improvement of the low-end gnss/ins systems for land vehicles navigation. *Mathematical Problems in Engineering*, 2013, 07 2013. DOI: 10.1155/2013/435286.

[9] P.S. Maybeck. *Stochastic Models, Estimation, and Control*. ISSN. Elsevier Science, 1982.

[10] Sebastian Thrun. *Probabilistic Robotics*. The MIT Press, Cambridge, Massachusetts, 2005.